3-2 $^{40}Ca^{+}$ Ion Optical Frequency Standard

MATSUBARA Kensuke, LI Ying, NAGANO Shigeo, KOJIMA Reiko, KAJITA Masatoshi, ITO Hiroyuki, HAYASAKA Kazuhiro, and HOSOKAWA Mizuhiko

Optical frequency standard using ion traps was proposed for the first time by H. Dehmelt in the 1980's. NICT started investigations using this technique at the age of the Radio Research Laboratory (RRL), and the development of an optical frequency standard using calcium ions was started in 2004. As a result of simultaneous successful developments of an optical comb frequency counter and an ultra-narrow linewidth clock laser system, we attained a frequency uncertainty of 1.2×10^{-14} and an Allan deviation about 5×10^{-15} at 100 seconds in 2009. We have recently developed an ion trap system equipped with a magnetic shield in order to decrease the environmental magnetic field fluctuation. We have measured the clock transition spectrum with the linewidth of about 60 Hz, which is the fifth part of the previously measured linewidth. We are presently focusing on measurements of the clock transition frequency with the aim of achieving uncertainties of the 10^{-15} level.

Keywords
Optical frequency standard, Ion trap, Calcium ion, Electric quadrupole transition

1 Introduction

Optical frequency standards utilizing single trapped ions or neutral atoms in the optical lattice are currently being development worldwide. Its main goal is to construct new frequency standards that surpass the current primary frequency standard making use of the microwave transition of cesium atoms (approx. 9.2 GHz) in terms of accuracy. At the same time, by applying their ultimate precision studies for measuring extremely minute temporal changes of physical constants are also gathering attention. Optical frequency standards that are possibly applicable to the sophistication of global positioning technologies are currently under competitive development over the world.

The optical frequency standard based on a single ion was proposed by Dr. Dehmelt in the early 1980's[1]. Its advantages are: (1) Enabling high-precision frequency measurement without the first-order Doppler broadening by using the laser cooling; (2) Enabling ample decrease of spectral broadening due to the Fourier limit by lengthening interaction time between electromagnetic waves and ions; (3) Enabling measurements that have full control over interactions with the surroundings utilizing one or a small number of ions in a vacuum[2]. Compared with the optical lattice type of optical frequency standard, the ion trap type has a disadvantage of a small number of particles that can be observed simultaneously. Still, from the viewpoint of the advantage of (3) in particular, studies for optical frequency standard using ions as the method for obtaining frequencies with the world's highest accuracy, as of drafting the present article, are carrying on[3]. In recent years, high-performance lasers with the spectral broadening narrowed to the 1 Hz level have appeared, and furthermore, ever simpler and more highly precise optical frequency measurements owing to optical combs are widespread, which are being examined aimed

at various applications.

The ions with the electronic configuration of alkali metals such as Ca^+, Sr^+, Yb^+, Hg^+ have been put in use for the ion-trap type of frequency standards[4]-[7]. Having been readily subject to laser cooling using laser radiations or their second harmonics, they can establish frequency standards employing electric quadrupole transitions. In recent years, the electronic configuration of alkaline earth metals such as In^+ and Al^+ are also adopted[8]. Some contrivances to apply laser cooling to them are required; still, they can realize the ultimate frequency standard with an accuracy of the 10^{-18} because uncertainty in transition frequencies caused by black-body radiation is very small. In comparison between transition frequencies of two Al^+ ions, the world highest frequency accuracy of 8.6×10^{-18} has been so far reported[3].

National Institute of Information and Communications Technology (NICT) has been pursuing the basic research for the ion trap and its application to frequency standards since the primary frequency standard of the microwave region was under development. In recent years, NICT has been developing optical frequency standard with calcium ions ($^{40}Ca^+$). In 2009, it reported a transition frequency of calcium ions with an uncertainty of the 10^{-14} level which was contributed to updates of the list of standard frequencies recommended by the Consultative Committee for Time and Frequency, the International Committee of Weights and Measures[9].

The present article will report from the principles of ion trap to the construction of optical frequency standard and the current progress as well.

2 Ion trap

2.1 Principle of ion trap

The ion trap is a device to confine ions to the micro space in the electromagnetic field. Upon the satisfaction of several conditions, ions can be confined to a range fully shorter than the optical wavelength used for frequency standard. Among several types, we will discuss the Paul trap[2][10]. The basic Paul trap consists of one ring electrode and two end-cap electrodes in the shape of hyperboloid of revolution as shown in Fig. 1.

Apply electrostatic potential V_{DC} to between the ring and the end-cap electrodes; then potential ϕ occurs as is expressed by:

$$\phi = \frac{V_{DC}}{r_0^2 + 2z_0^2}(r^2 - 2z^2) \qquad (1)$$

Here, with use of cylindrical coordinate system (r, z), r_0 $(=\sqrt{2}z_0)$ denotes the internal radius of the ring electrode. Potentials only by electrostatic potential has no minimum point (Earnhow's Theorem), and thus the potential in Equation (1) cannot trap ions. Apply $V_{AC}\cos\Omega t$ instead; then inward and outward forces occur to ions alternately in each direction of r and z. Integrate it with one cycle; then ions would receive inward force to be trapped by pseudopotential Φ that is expressed by:

$$\Phi = \frac{Q_{ion}V_{AC}^2}{m\Omega^2(r_0^2 + 2z_0^2)^2}(r^2 + 4z^2) \qquad (2)$$

Q_{ion} and m denote charge and mass respectively. Mathieu's equation expresses more precise motions of ions. Apply the potential expressed by $V = V_{DC}+V_{AC}\cos\Omega t$ to between electrodes and set $\tau = \Omega t/2$; then it is expressed by:

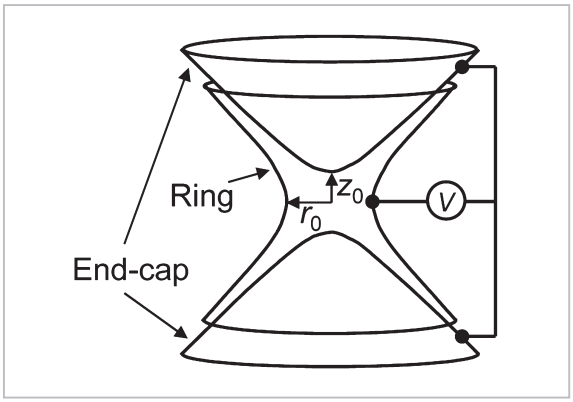

Fig.1 *Ion trap*

The trap electrodes consist of three hyperboloids of revolution taking Z direction as axis, and high voltage is applied to between the electrodes.

$$\frac{d^2u_i}{d\tau^2} = (a_i - 2q_i\cos 2\tau)u_i = 0, \qquad (i = r, z)$$
$$a_z = -2a_r = -\frac{16Q_{ion}V_{DC}}{m\Omega^2(r_0^2 + 2z_0^2)}, \quad q_z = -2q_r = \frac{8Q_{ion}V_{AC}}{m\Omega^2(r_0^2 + 2z_0^2)} \tag{3}$$

Solutions for Equation (3) become constrained motions when a_z and q_z are in a certain range, and in case of $a_z < q_z \ll 1$, solutions denoting motions can be approximated as:

$$r_i(t) = r_i\cos(\omega_i t + \phi_i)\left\{1 + \frac{q_i}{2}\cos(\Omega t)\right\}$$
$$\omega_i = \beta_i\frac{\Omega}{2}, \quad \beta_i = \sqrt{a_i + \frac{q_i^2}{2}}, \qquad (i = r, z) \tag{4}$$

In Equation (4), ion motion can be regarded as the motion that is harmonic oscillation with small amplitude and a frequency of Ω (micro motion) being added to harmonic oscillation with large amplitude and a frequency of ω_i (secular motion).

2.2 Laser cooling of ions

Since a newly trapped ion has a large kinetic energy, Doppler broadening is too large to measure the transition with a high resolution. That is why the laser cooling is adopted. Leaving details of laser cooling to another publication[2], we will here give an explanation for the Doppler cooling from the viewpoint of energy. Consider an energy level system composed of two states, where an ion is pumped up a single excited state from the ground state by optical irradiation, and from the excited state it decays only to the ground state by spontaneous emission. In general electric dipole transitions, ions repeat excitation and emission approximately 10^8 times per second. With the use of a laser traveling in the opposite direction of the motion direction of ions, the Doppler effect makes the energy of photons (frequency of light) absorbed by moving ions smaller than that absorbed by standstill ions. When the ions emit photons by spontaneous emission, the energy of photons varies being dependent on relation between the motion directions of ions and photons. By the spontaneous emission, photons are emitted in the random directions. Now, taking average of multiple times of spontaneous emission, the energy of emitted photons accords with the energy (frequency) of photons emitted by standstill ions. Therefore, by a single excitation and spontaneous emission, ions lose the energy, when averaged, corresponding to the energy difference between the frequency of irradiating laser and the frequency by which the standstill ions are excited. The repetition of this process cools ions as far as an ultralow temperature.

However, at an ultralow temperature, the energy change corresponding to the recoil energy becomes impossible to ignorable in each cycle of absorption and emission of photons, which limits the achieving temperature to approximately 1 mK.

Ions being trapped are reciprocating in each direction of *r* and *z* as is shown in Equation (4). Therefore, ions can be cooled with the single laser only traveling in one direction having the components of both *r* and *z*; in principle, it is easier than neutral atoms which require laser radiation from six directions. Then, when ions nearly stop by cooling, the Doppler broadening of spectrum disappears to result in the emission of strong fluorescence. For laser cooling by electric dipole transition, when radiating the laser of saturation power on ions, a single ion emits approximately 10^8 photons per second. Then, even fluorescence detection at an efficiency of 10^{-4} enables to detect about 10^4 photons. On account of that, fluorescence from only one trapped ion can be detected at enough *S/N* ratios. Figure 2 shows the spectrum at the laser cooling of singly trapped $^{40}Ca^+$ ion. Here, ions undergo laser cooling and emit fluorescence only at frequencies lower than resonant frequency (i.e., frequency which is resonant with standstill ions). At higher frequencies, on the other hand, a large Doppler broadening arises to almost negate fluorescent intensity because ions are given energy from the laser and heated, which is shown by an unsymmetrical spectrum in Fig. 2. In the measurement given in Fig. 2, one can estimate the temperature of cooled ions at a few mK from the spectral linewidth.

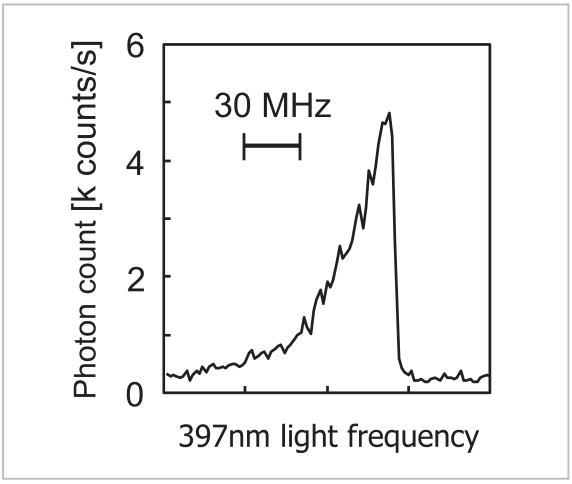

Fig.2 *Laser cooling of single Ca^+*

Laser-cooled ions emit strong fluorescence in a slightly longer wavelength than resonant frequency.

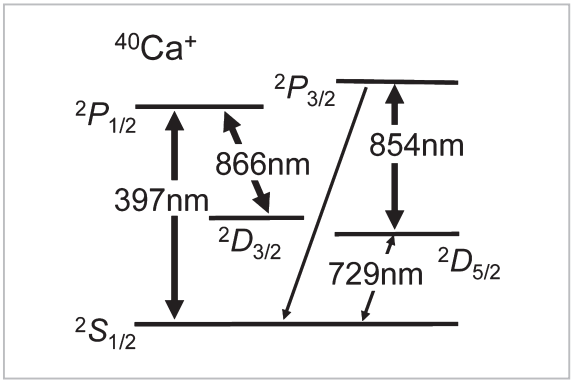

Fig.3 *Ca^+ energy levels*

Any wavelength in the figure enables photoexcitation using LD.

3 Clock transition and measuring equipments

3.1 Clock transition of calcium ions

Figure 3 shows the energy levels of a $^{40}Ca^+$ ion. Here, the $^2S_{1/2}-{}^2D_{5/2}$ transition is called the electric quadrupole transition, which is excited through interaction between $^{40}Ca^+$ ions, which locates in a sufficiently smaller area than the light wavelength, and the electric field gradient occurring from the optical phase difference in the space. Its probability is around a billionth of regular optical transitions (electric dipole transitions), and the $^2D_{5/2}$ state has the lifetime of approximately one second as a meta-stable state. In general, frequency standards with high accuracy and stability need transitions with a sufficiently narrow linewidth. The $4^2S_{1/2}-3^2D_{5/2}$ transition of $^{40}Ca^+$ ions has a natural width of some 0.2 Hz. Thus, we have adopted it as the transition used for frequency standards, i.e. clock transition. For this ion, the $^2D_{5/2}-{}^2P_{3/2}$ transition is utilized so as to immediately return the ion back to the $^2S_{1/2}$ state from the $^2D_{5/2}$ state.

In an attempt to observe the clock transition with a narrow linewidth, the laser cooling employing the $^2S_{1/2}-{}^2P_{1/2}$ transition is carried out for $^{40}Ca^+$. Since a transition is possible to proceed from the $^2P_{1/2}$ state to the $^2D_{3/2}$ state, the $^2D_{3/2}-{}^2P_{1/2}$ transition with a wavelength of 866 nm is simultaneously excited as well. Fully cooled ions are confined in a quite narrow region that is close to the lowest vibration state at the minimum of potentials in the ion trap. When this is distinctly smaller than the optical wavelength (Lamb-Dicke condition), the phase modulation of the optical electric field due to ionic motions becomes extremely small to get disappearance of the first-order Doppler broadening of linewidth. The linewidth of ionic transition satisfying the Lamb-Dicke condition is determined, if the natural width is sufficiently small, by the laser spectral and saturation linewidths, fluctuations in the electric and magnetic fields, etc. If these are appropriately under control to supply an adequately narrow linewidth, its spectrum is available for a frequency standard.

3.2 Experiment equipment

Figure 4 shows the experimental configuration. It comprises an ion trap, a light source for laser cooling and a clock laser; otherwise, it uses light source for photo-ionization of Ca atom, a femtosecond optical comb frequency counter and a microwave frequency standard, which are omitted for brevity from the figure. The present Special Issue contains articles on the clock laser, the optical comb frequency counter and the microwave frequency standard each. The ion trap is installed in the vacuum

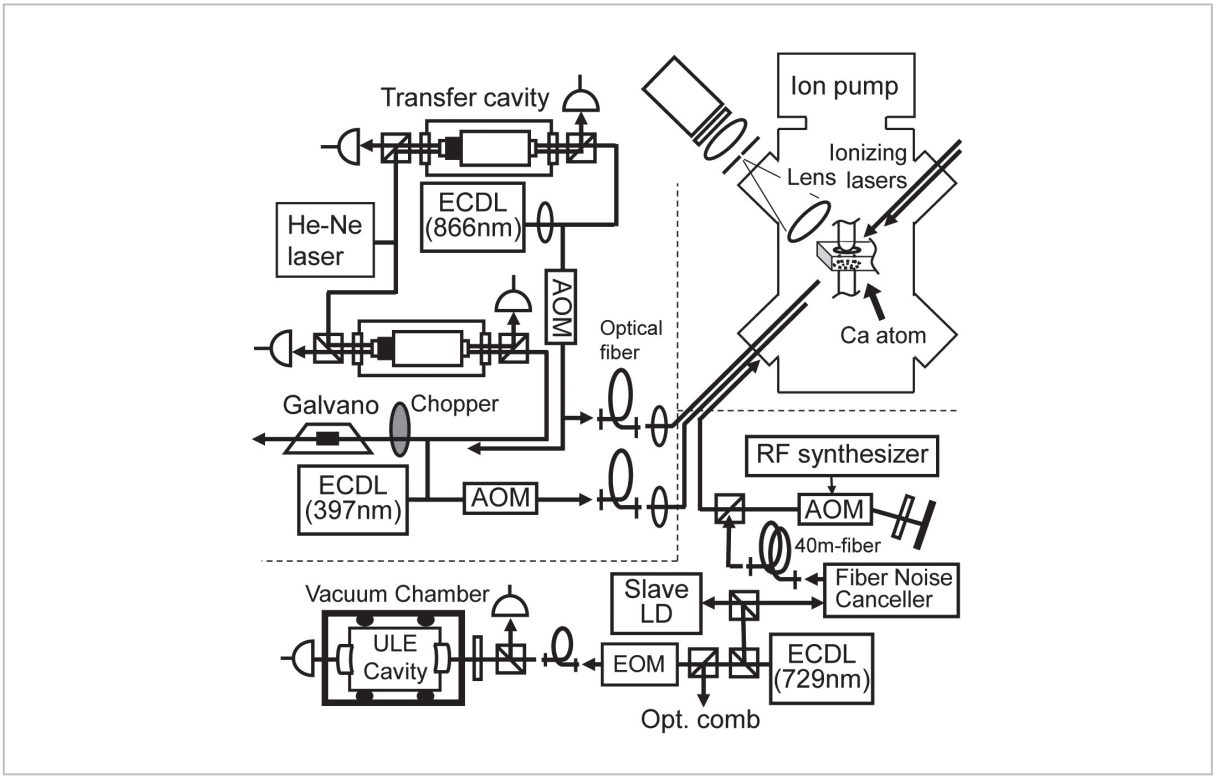

Fig.4 *Experimental setup*

EDCL: external cavity diode laser, AOM: acoustro-optical modulator, EOM: electro-optical modulator , ULE cavity: ultra-low-expansion cavity , Galvano: Galvano tube. PMT: photo-multiplier tube.

chamber where a vacuum degree of 5×10^{-8} Pa or so is maintained. The trap is composed of a ring electrode with a hole being 1mm in diameter and two rod electrodes, and applied an RF voltage of 23 MHz and 600 $V_{p\text{-}p}$ onto the ring electrode. The optical ionization of a calcium atom employs the 423 nm light that is obtained with the second harmonic generation using a periodically poled KTP crystal from a LD with a wavelength of 846 nm and the 376 nm light from an ultraviolet LD[11]. When more than two ions are trapped, they are reduced to a single ion by temporarily shallowing potentials of trapping, etc. And, the electric field is compensated with compensation electrodes installed near the trap. This compensation should lead to adequate cooling of ions, remove of ionic micro-motions due to electric field distortions and thus fulfillment of the Lamb-Dicke condition. Then, the cooled ions are irradiated with the clock laser of 729 nm to observe the clock transition.

3.3 Laser source

Here, we will discuss several lasers that were used for the measurement. For laser cooling, the laser diodes (LD) of 397 nm and 866 nm were adopted with the external cavity in the Littrow configuration (ECLD). One ECLD for 866 nm was a marketed product (Toptica), and we made the other for 397 nm from LD elements (Nichia Corp.) on our own. Having radiated the lights from these lasers together with that from the stabilized He-Ne laser (Melles Griot, currently CVI Melles Griot) into the Fabry-Pérot cavity, which was used as a transfer cavity, we stabilized the LD wavelength with reference to the wavelength of the He-Ne laser. In this manner, the frequency fluctuation being decreased at less than 2 MHz, an Allan standard deviation of 10^{-10}@1–10^{3} s was confirmed[12]. This ensures a sufficient stability since an electric dipole transition with a natural width of several MHz or larger is used for laser cooling.

Regarding the 729 nm clock laser for observing clock transitions, Y. Li et al. have released a detailed report in this Special issue[13]; so we only provide an outline here[14]. Commercial LD elements were used in the Littman external-cavity-configuration. Output was amplified up to 18mW by the injection locking into the slave LD. Simultaneously, optical frequencies were stabilized by the high-finesse optical cavity of Ultra-Low-Expansion (ULE) to achieve a narrow linewidth and high stability. The ULE optical cavity has a quite small change of cavity length and coefficient of thermal expansion. Additionally, in order to prevent changes in temperature and vibrational impacts, the ULE cavity was put in a double-layer copper pipe coated with gold, and then positioned in the chamber of a vacuum degree of 10^{-6} Pa. The chamber was placed on the vibration isolated table (Minus-K), and the whole device was set in the sound insulation box. The ULE cavity has a temperature, at which the coefficient of thermal expansion becomes zero (zero-expansion temperature) and the resonant frequency undergoes no change in spite of change in temperature. We measured it and maintained the temperature at 1.50 ± 0.01 °C by force of Peltier elements. Laser frequency was stabilized to the ULE cavity by the Pound-Drever-Hall technique. The spectral width of 3 Hz or lower was confirmed from the frequency beat of two independent clock lasers. And so was the frequency stability of the 10^{-15} s for 10 seconds by measurements using the cryogenic sapphire oscillator (CSO) as a reference.

The light stabilized by the ULE cavity was transmitted to the ion trap through the polarization-maintaining single-mode fiber with 40m length. On this occasion, fiber vibrations and temperature changes cause phase noise in light. In order to cancel this, an acoustro-optical modulator (AOM) was inserted between the fiber and the clock laser, and then part of the output from the fiber was returned by the partial reflection mirror. After measuring the frequency difference (beat) of the lights going and returning through the fiber, we divided it in half to set as the error signal to control the drive frequency of AOM[15]. This method successfully curtailed the noise in the band below about 2 kHz. Meanwhile, as a result of measuring the frequency difference (beat) outside the feedback loop, it was shown that the phase noise fell below the device resolution (1 Hz), which assured a sufficient denoising.

4 Measurement of absolute transition frequencies

4.1 Measurement of clock transition spectrum

The electron-shelving technique is employed for measurement of clock transition spectrum[1]. During the laser cooling process, the ions repeat the $^2S_{1/2}-{}^2P_{1/2}$ transition, so frequently that fluorescence is observable at a sufficient *S/N* ratio even from a single ion. Here, once a clock transition occurs with the clock laser, after transition, a single ion remains in the $^2D_{5/2}$ state (or gets shelved); in the meantime, fluorescence cannot be detected. This method makes it possible to observe a clock transition with an extremely small transition probability at almost perfect detection efficiency. The shelving frequency depends on the clock laser frequency. Thus, if one measures the shelving frequency while changing the clock laser frequency, they can observe the transition spectrum of clock transition.

When the strong $^2S_{1/2}-{}^2P_{1/2}$ transition is excited, the energy of the $^2S_{1/2}$ state changes, and consequently, the transition frequency of clock transition varies (or the light shift). For the sake of preventing it, in our measurements, we suspended the irradiation of cooling light after completing laser cooling and irradiated clock laser for a certain time. If fluorescence cannot be detected when thereafter irradiating the cooling lasers again, it turns out that ions have been shelved to the $^2D_{5/2}$ state or the immediately-preceding irradiation of clock laser has caused a clock transition. On the contrary, if fluorescence can be detected, it suggests that there has been no clock transition. After judging whether a clock transition canses, ions are returned to the laser cooling cycle by the 854-

nm light. Meanwhile, commercially-available AC100 V here changes the magnetic environment at a frequency of 50 Hz. It causes an additional Zeeman shift to widen the spectral linewidth. Therefore, we synchronized the optical irradiation with the electric 50 Hz. Thus, the transition spectrum was observed in the magnetic environment with changes constrained.

Measurements proceed adding a stable static magnetic field (approx. 80 μT this time). Since the Zeeman splitting being symmetrical in positive and negative occurs to a clock transition, the transition frequency with the first-order Zeeman shift compensated was obtained by measuring the center frequency of the Zeeman splitting. Figure 5 shows an example of spectrum. In order to obtain one of the transition probability data (black dots in Fig. 5), after fixing the clock laser frequency, the cycle consisting of three steps was repeated 100 times: the laser cooling, the irradiation of clock laser and the probe of clock transition. The measured number of clock transitions divided by the number of cycles (100 here) was calculated as the transition probability at that clock laser frequency. The more the cycle number increases, the better spectral *S/N* ratio improves; still, in the meantime, the clock laser frequency drifts leading to an increase in the uncertainty of transition frequency. Then, we determined the cycle number taking the drift speed into consideration. And, as will be discussed in **4.2** below, aimed at compensation of quadrupole shifts being different between magnetic sublevels, the following four transition spectra were measured 50 times each: ($^2S_{1/2}$, $M_j = -1/2 \rightarrow {}^2D_{5/2}$, $M_j = -3/2$), ($^2S_{1/2}$, $M_j = 1/2 \rightarrow {}^2D_{5/2}$, $M_j = 1/2$), ($^2S_{1/2}$, $M_j = -1/2 \rightarrow {}^2D_{5/2}$, $M_j = -1/2$), ($^2S_{1/2}$, $M_j = 1/2 \rightarrow {}^2D_{5/2}$, $M_j = 3/2$).

Furthermore, in each of 50 measurements, having acquired one of the data (black dots in Fig. 5) and then changed transitions as ($M_j = -1/2 \rightarrow M_j = -3/2$), ($M_j = 1/2 \rightarrow M_j = 1/2$), ($M_j = 1/2 \rightarrow M_j = 3/2$), and ($M_j = -1/2 \rightarrow M_j = -1/2$) in order, peaks of the four spectra were observed in as short time as possible. Irradiation time of the clock laser was set as 4 millisecond for one time. In this case, the linewidth of some 200 Hz corresponds to the Fourier limit. A linewidth sufficiently narrower than 300 Hz could not be observed even for a longer irradiation time of the clock laser. It is supposed that the linewidth has been broadened on account of fluctuations

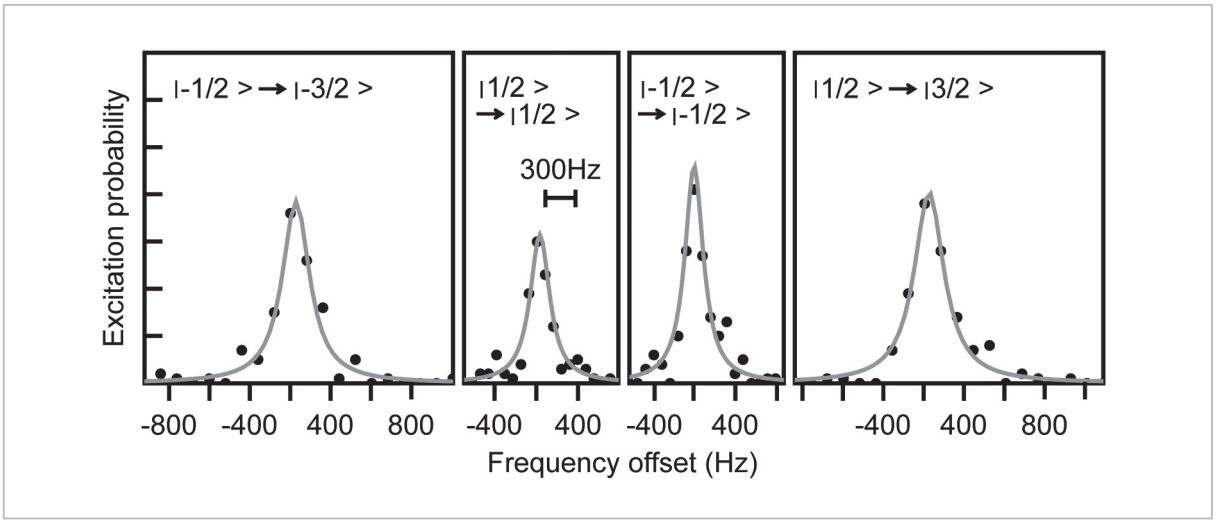

Fig.5 *Zeeman spectrum*

In a stable magnetic field of approx. 80μT, we observed two pairs of Zeeman components: ($^2S_{1/2}$, Mj = −1/2 → $^2D_{5/2}$, Mj = −3/2), ($^2S_{1/2}$, Mj = 1/2 → $^2D_{5/2}$, Mj = 1/2), ($^2S_{1/2}$,Mj = −1/2 → $^2D_{5/2}$, Mj = −1/2), ($^2S_{1/2}$, Mj = 1/2 → $^2D_{5/2}$, Mj = 3/2). The transition spectrum of | ± 1/2 > →| ± 1/2 > has a linewidth of about 300Hz. The transition of | ± 1/2 > →| ± 3/2 > was observed as having a linewidth of approx. 400Hz since the coefficient of the primary Zeeman shift accounts for double the transition of | ± 1/2 > →| ± 1/2 >.

in the environmental magnetic field during the irradiation time. This will be discussed in **6** below.

4.2 Estimation of frequency shifts

An absolute frequency of a transition must be determined on the condition of no-perturbation. Thus, it is necessary to compensate from measured transition frequencies frequency shifts that are caused by perturbations in experiments. We discussed the compensation of the first-order Zeeman shift in **4.1** above. While laser cooling was suspended at time of irradiation of the clock laser, AOM to be used as a shutter slightly passes light even at time of cut-off. In order to compensate frequency shifts by this light, we performed laser cooling at several light intensities in observing the clock transition spectra and estimated the transition frequency when the optical intensity of laser cooling becomes zero. Moreover, the quadrupole shift (5 Hz or less in general) is a frequency shift that occurs in the clock transition. This is the shift caused from interaction between the electric field gradient at the position of the ion and the $^2D_{5/2}$ state, and is difficult to theoretically estimate. Its shift amount varies due to changes in the electric field gradient even during an experiment. There are two methods for compensation of quadrupole shifts: adding the magnetic field from each of three orthogonal directions to average the clock transition frequencies measured, or measuring transition frequencies to levels with different magnetic quantum numbers (M_j) in the $^2D_{5/2}$ state to compensate by the dependence of shifts on magnetic sublevels[16]. The latter was used for this time; we measured transition frequencies to four levels of the $^2D_{5/2}$ state: M_j= ±1/2 and ±3/2, and then compensate the quadrupole shift $\Delta\nu_Q$ with the following equation:

$$\hbar\Delta\nu_Q = \frac{J(J+1)-3M_j^2}{J(J+1)} \times A\,,\ A = \frac{1}{4}\frac{dE_z}{dz}\Theta(D,J)(3\cos^2\beta - 1)\,, \quad (5)$$

Here, Θ (D, J) stands for quadrupole moments, and β for the angle between the magnetic field and the quantum axis. Equation (5) clarifies that mass ratio of the quadrupole shift of the $^2D_{5/2}$ state to the M_j = ±1/2 level to the ±3/2 level shift is 4 to 1. Since the quadrupole shift temporally varies, it is necessary to estimate the shift amount from the spectrum that has been measured in a short time. At each of 50 times of measurement, the full width at half maximums of four transitions has been measured in a short time (within five minutes). At each of 50 times, we calculated transition frequencies with the first-order Zeeman shift compensated from the pair of transitions to M_j = ±1/2 and that to ±3/2 each. Then, supposing that the difference between these two transition frequencies has arisen out of the quadrupole shift shifting at the mass rate of 4 : 1, we calculated the shift amount and estimated measured values for transition frequencies with the quadrupole shift compensated: 50 measured values for 50 times of experiment. The measured quadrupole shift of the ($^2D_{5/2}$, M_j = ±1/2) levels was 1.9 Hz on average. The standard error, i.e. the standard deviation of measured values divided by the square root of the number of measurement (here 50), was 3.4 Hz. This error is chiefly caused from the variation in measured values that are estimated from a linewidth of about 300–400 Hz. Temporal change in the quadrupole shift during the experiment could not be observed. Apart from these, the gravity shift was estimated at 3.4 (±0.1) Hz by measuring the altitude of the laboratory[17], and the black-body radiation shift at 0.4 (±0.1) Hz[18] based on theoretical calculation. In addition, the second-order Zeeman shift, the drift of the static magnetic field due to changes of the coil current during measurement, and uncertainty for measured frequencies due to the frequency drift of the clock laser were each estimated at 0.2 Hz or less. Other frequency shifts such as the second-order Doppler shift were estimated as sufficiently small for the level of uncertainty that was obtained this time.

4.3 Determination of absolute transition frequency

At each of 50 times of spectral measurement, we calculated transition frequencies

with the first-order Zeeman shift compensated, and so with the quadrupole shift and the light shift caused form cooling laser compensated. Figure 6 shows as a histogram the distribution for measured values of the transition frequency after compensation. The clock laser frequency was measured with use of the optical comb frequency counter which NICT has developed with the mode-locked femtosecond Ti:S laser[19]. For the reference frequency of the optical comb system and frequency modulation of the lasers, 10 MHz of the hydrogen maser of NICT was put in use. The hydrogen maser frequency is compared with UTC (NICT) or the standard time at NICT every hour[20]. Furthermore, making use of the report on the difference between the standard times of each country and the International Atomic Time that is announced by the International Committee of Weights and Measures (Circular T)[21], we determined the clock transition frequency based on the definition of the second of SI units. From the frequency data in Fig. 6 and the frequency calibration using UTC (NICT) and Circular T, as well as from compensation of the systematic shifts, the absolute frequency of the clock transition was determined at 411 042 129 776 395 Hz. Uncertainty was evaluated at ±4.8 Hz, and the relative ratio to transition frequency was 1.2×10^{-14}. The frequency measurement for the $^{40}Ca^{+}$ clock transition was conducted by our group in 2008[3], and by the Innsbruck University, Austria in 2009 (the measured value was 411 042 129 776 393 (±1) Hz)[22]. Following these, in 2009, the Consultative Committee for Time and Frequency, the International Committee of Weights and Measures recommended the frequency as 411 042 129 776 393 Hz (an uncertainty of 4×10^{-14})[9]. In 2008, we observed the clock transition with a linewidth of about 500 Hz to obtain an uncertainty of transition frequency of 4.4×10^{-14}[3]. The uncertainty became small this time, and in addition, the determined value at this time agreed to the recommended value that was provided by the Consultative Committee for Time and Frequency in 2008.

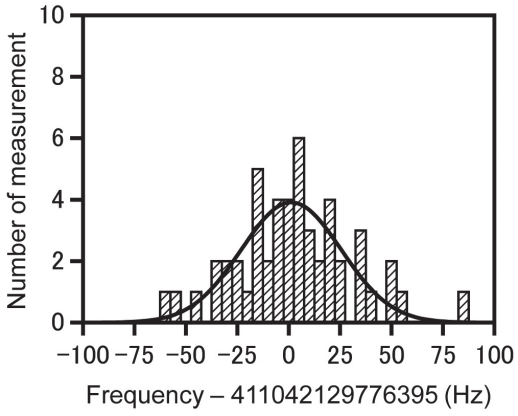

Fig.6 *Histogram for transition frequencies*

Spectrum was measured 50 times, provided frequency calibration for each to be made the distribution of absolute frequencies. Standard variation is 28.6Hz and that of the center value is 4.1Hz.

5 Long-term frequency stabilization of clock laser

5.1 Long-term stabilization of laser

In order to apply the transition frequency measurement to the optical frequency standard, it is necessary to control optical frequency generators such as lasers by using the transition frequency, and to compare that with other frequencies. Then, to confirm its performance as an optical frequency standard, the clock laser frequency was stabilized with the $^{40}Ca^{+}$ ion transition, and its stability was evaluated. Figure 7 illustrates the system for this evaluation[23]. In the short term, the clock laser frequency (f_{LD} in Fig. 7) is fully stabilized with the ULE cavity, while in the long term, it slowly drifts by aging of cavity length. An AOM for compensating such long-term drift (expressed as "AOM1") was added to an AOM for observing clock transitions (so as "AOM2"). Here, we observed the transition only to the ($^2D_{5/2}$, $M_j = \pm1/2$) levels taking no account of variation in the quadrupole shift because it has little influence on stability. Having shifted the optical frequency with AOM2, we repeatedly measured transition probabilities in six clock-laser frequencies: two frequencies being clos-

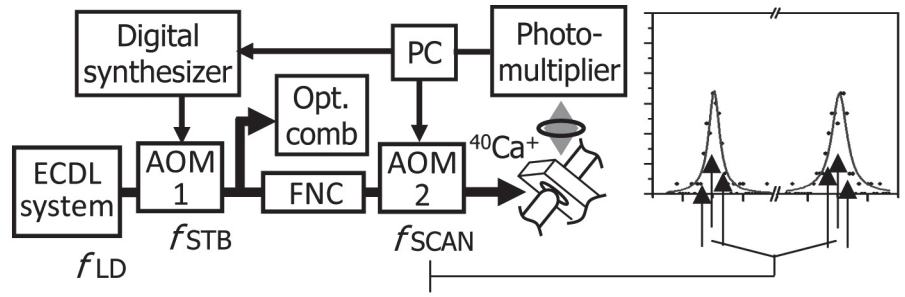

Fig.7 *Key map for stabilization*

The center value of frequency to be switched with AOM2 is stabilized.
The frequency of AOM1 (f_{STB}) is adjusted so that the sum of center frequencies of ECDL (f_{LD}), AOM1 (f_{STB}) and AOM2 (f_{scan}) can be stabilized to the center frequency of the Zeeman effect.
FNC: fiber noise cancellation device

est to the peaks of the two transitions, and four frequencies being distant positively and negatively from the closest to the two peaks by half of the full width at half maximum (FWHM). The FWHM is adjusted as needed so that the ratio of transition probabilities at the FWHM to that in the closest to the peak can near 2 to 1. Moreover, the balance of transition probabilities in two frequencies distant by the FWHM is detected at each of the two transitions, and the frequency shifts with AOM1 and AOM2 are controlled so that two transition probabilities there can equal out[23]. Here, we fixed the center value of frequency shifts of AOM2 switching the six frequencies (f_{SCAN} in Fig. 7). Instead, we adjusted frequency shifts with AOM1 (f_{STB}) to make the sum of $f_{LD} + f_{STB}$ and fixed center of f_{SCAN} equal to the clock transition frequency with the first-order Zeeman shift compensated. Since the center value of the frequency shift of AOM2 is fixed, the long-term variation in the clock laser frequency (f_{LD}) are compensated by the frequency of AOM1 (f_{STB}) and its sum frequency is stabilized. That stabilized frequency was measured with the optical frequency comb.

5.2 Stability measurements and the Allan standard deviation

Figure 8 shows the measured Allan standard deviation. Black circles in the figure denote frequency stabilities when f_{STB} is compensated every 100 seconds using observational results of clock transition frequency from 500 seconds earlier. Black squares denote stabilities of the clock laser frequency that has been stabilized with the ULE cavity. Black triangles denote CSO stabilities compensated with a hydrogen maser that has been used as reference

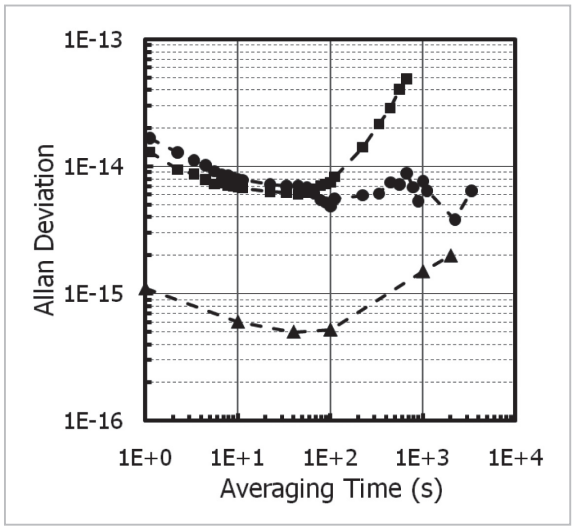

Fig.8 *Allan standard deviation*

■: Stability of the clock laser stabilized with the ULE cavity
●: Stability resulted from further stabilization, with the transition of Ca^+ ion, of the frequency of the clock laser that has been stabilized with the ULE cavity
▲: Stability of a cooled sapphire oscillator calibrated with the hydrogen maser that has been used for reference to frequency comparisons

for the measurements. Because of a drift of the ULE cavity length, stability of the clock laser frequency (f_{LD}) starts deteriorating at an averaging time of around 100 seconds. View black circles; then it turns out that the use of $^{40}Ca^{+}$ ions have improved the long-term stability, securing a stability of approximately 5×10^{-15} at an averaging time of 100 seconds. However, stability has not been improved better at over 100 seconds. This phenomenon hints that frequencies to be measured may contain flicker frequency noise[24]. While we have not been able to identify the noise source so far, we needed to take measures against the possibility of irregular variations in the magnetic field that could occur at long time intervals.

6 Development of ion trap chamber with magnetic shield

6.1 Magnetic environments in laboratory

As was discussed in **4**, in the previous measurements, the clock laser irradiation was synchronized with AC100V 50Hz to constrain the influence of changes in the environmental magnetic field. With consideration for the Fourier limit, observations of clock transitions with as narrow a linewidth as possible necessitate as long an irradiation time as possible. The longer the irradiation time, the more magnetic field variations grow to expand the linewidth. In Fig. 5, the Fourier-limit linewidth amounts to approximately 200 Hz with the clock laser irradiation for 4 milliseconds. Assume that the square of the observed linewidth is equal to the sum of the square of each causal line broadening; then there is considered to be an additional line broadening of nearly 200 Hz, except the Fourier limit, for the observed linewidth of approximately 300 Hz in the $|\pm 1/2> \rightarrow |\pm 1/2>$ transition. Supposing magnetic field variations as the main trigger for such additional broadening, we measured the magnetic field around the ion trap with the 3-axis magnetic field sensor. As a result, we observed a magnetic field variation with an amplitude of some 0.2 μTp-p that was synchronized with AC100V 50Hz. The magnetic field variation of 0.2 μTp-p broadens the spectrum of the $|\pm 1/2> \rightarrow |\pm 1/2>$ transition by 1 kHz or so. Assume that the additional 200 Hz broadening in the $|\pm 1/2> \rightarrow |\pm 1/2>$ transition was caused by magnetic field variations; then it turns out that its effect was reduced to be smaller than 20 % in manner of synchronization with AC100 V. Also, as is shown in Fig. 9, an irregular variation of DC magnetic field was observed in the Z (vertical) direction at maximum 0.1 μT or so. This is chiefly due to the influence of the railway being distant from the laboratory by some 1 Km. In this measurements, since a static magnetic field of approximately 80 μT was added to the horizontal direction (X direction in Fig. 9), the influence of magnetic field variations in the vertical direction onto the composed magnetic field has become small. Although it is considered that magnetic field variations shown in Fig. 9 gives no systematic shifts to the transition frequencies that have been determined in the eight-hour long experiment, it is still necessary for frequency measurements at higher accuracy in future to further do away with influence from environmental magnetic field fluctuations. There are generally two methods for inhibiting

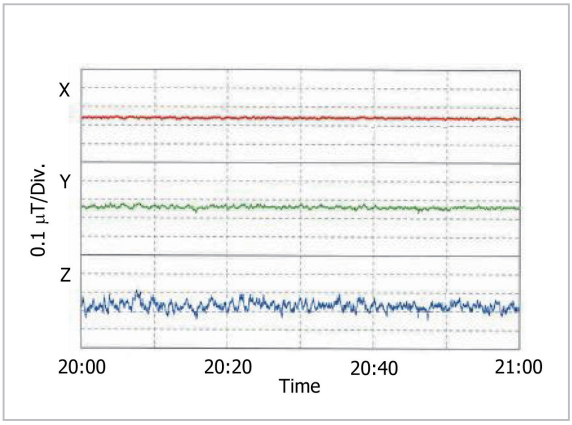

Fig.9 *Fluctuations in DC magnetic field*

An example of fluctuations in the environmental magnetic field at around the ion trap (20:00–21:00). X is the direction adding the static magnetic field to ions, and Z is the vertical direction. DC magnetic field variations in X, Y and Z directions in the middle of the night (2:00–4:00) without any train operation. Measured by Ohtama, Co., Ltd.

fluctuations in environmental magnetic fields. One is to shield the ion trap from environmental magnetic fields with a magnetic shield. The other is to adjust the current in a 3-axis Helmholtz coil so as to negate magnetic fluctuations. Among these, we decided to adopt the magnetic shield that can unfailingly constrain magnetic fluctuations in a small area.

6.2 Magnetic shield performance and clock transition observation

We planned to observe a linewidth of less than 100 Hz by means of installing a magnetic shield. For instance, set the irradiation time of clock laser at 20 milliseconds; then the Fourier limit will amount to approximately 40 Hz. At this time, if the broadening due to external magnetic fields can be controlled down to about 50Hz, one can expect the clock transition with a full width at half maximum of about 70 Hz. The irradiation time of 20 milliseconds will corresponds to one cycle of 50 Hz, and thus the linewidth cannot be constricted by synchronizing with AC100V. A line broadening of 50 Hz arises in a magnetic field variation of some 0.01 μT. In order to attenuate the measured 0.2 μTp-p variation to 0.01 μTp-p variation level, the magnetic field intensity needs to be set at 1/20 or below.

The shield was designed in collaboration with Ohtama, Co., Ltd. The vacuum chamber is equipped with the electrical wiring, the vacuum pluming and the glass window for optical incidence and detection, which should not be interfere with by shielding to be implemented. For conducting measurements in stable magnetic fields, three pairs of Holmheltz coils are installed inside the shield. We decided to make the shield out of permalloy board with 1 mm in thickness considering solidness and fabricability, and employed the double layer because of insufficiency of shielding effect with the single layer. Figure 10 shows a photo of the magnetic shield. While the vacuum chamber is a cube with 70 mm sides, the shield became a moderately-large cylinder with an external diameter and a shaft length both of approximately 300 mm. Table 1 shows shielding coefficients of the magnetic shield. The double layer procured much greater shielding effectiveness than the single layer. Shielding factor, depending on the frequency of magnetic field variations, reached over 25 at around 50 Hz and accordingly secured the specifications that can achieve its goal. Shielding effectiveness is produced a lot more in the perpendicular orientation than in the shaft orientation of the cylinder. Accordingly, the current installation method with the shaft oriented horizontally enables highly-ef-

Fig.10 *Photo of the magnetic shield*

The magnetic field is the cylindrical case in the right of the photo. The coil for the magnetostatic field and the vacuum chamber for trap are placed within the two-layered shield

Table 1 *Coefficients of magnetic shielding*

freq. (Hz)	2 layer		1layer	
	radius	axis	radius	axis
0.2	325	19	9	2
1	349	20	10	2
55	259	27	8	3
100	155	29	6	3
200	84	29	4	3
500	41	31	3	3

Coefficients are expressed by the value of the intensity without magnetic shield divided by the intensity with shield, and depend on the frequency of AC magnetic field. A profound effect was obtained with the two-layer; small effect in the axial direction of the cylinder, still the enough effect of more than 25 even at around 50 Hz.

fective shielding of a large DC magnetic field variation in the vertical orientation that was observed in Fig. 9.

We have so far succeeded in observing the clock transition by trapping a single $^{40}Ca^{+}$ ion in the ion trap placed inside the shield. The configuration of the ion trap is the same as that of previous ones. Figure 11 shows the observed clock transitions of ($^2S_{1/2}$, $M_j = 1/2 \rightarrow {}^2D_{5/2}$, $M_j = 1/2$) and ($^2S_{1/2}$, $M_j = -1/2 \rightarrow {}^2D_{5/2}$, $M_j = -1/2$). The irradiation time of the clock laser is set as 20 m second. The full width at half maximum was measured approximately 60 Hz. It can be considered that the magnetic shield well attenuated magnetic field variations and thus the linewidth could be constricted down to 1/5 as narrow as the previous ones. The Fourier limit due to the irradiation time can be estimated at 40 Hz, and the additional broadening at 45 Hz or so. It seems that the shielding effectiveness as roughly expected and thus the aimed linewidth were achieved.

7 Conclusions

7.1 Future measurements

The new development of the ion trap equipped with the magnetic shield enabled the observation of the clock transition with a linewidth of approximately 60 Hz. We are currently proceeding with frequency measurements in order to achieve an uncertainty of the 10^{-15} level. Assume that attainable uncertainty is inversely proportional to spectral Q values (values of transition frequency divided by the linewidth); then we can expect about one fifth of the existing uncertainty of 1.2×10^{-14}. However, because of uncertainty discussed in **4.2**, we cannot easily estimate any definitive uncertainty. Moreover, since Circular T described in **4.3** releases a report on frequency comparisons in terms of averages for every five days and thus cannot perform comparisons for the certain period of the measurement time of $^{40}Ca^{+}$ ions, we have so far taken an uncertainty of some 5×10^{-15} into consideration. Then, in order to obtain an uncertainty smaller than this value, frequency determination based on the Cs atomic fountain primary frequency standard being operated by NICT is required. We are presently planning measurements targeting the 10^{-15} uncertainty level. We are measuring a single $^{40}Ca^{+}$ ion in the ion trap. Thereby, measurements at a high speed should be conducted by minimizing the time for such things as changing clock laser frequencies. Moreover, since laser frequency drift led by changes in the ULE cavity length contains large components which are propor-

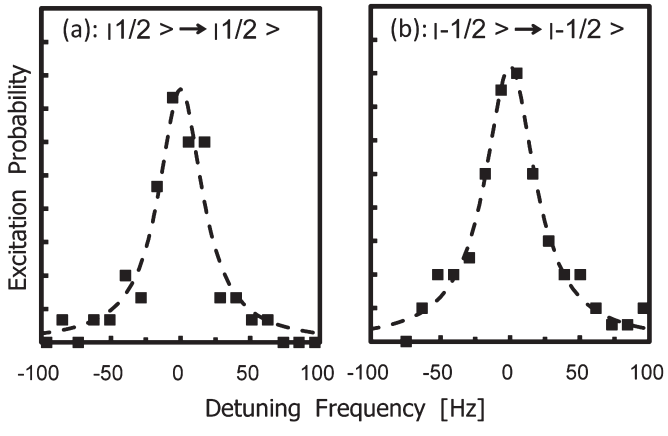

Fig.11 *Transition spectra using shield*

In the magnetic field with a stability of 60μT within the magnetic shield, a pair of Zeeman components of ΔMj=0 was observed; (a) is the transition of ($^2S_{5/2}$, Mj=1/2 →$^2D_{5/2}$, Mj=1/2), (b) is the transition of ($^2S_{5/2}$, Mj=−1/2 →$^2D_{5/2}$, Mj= −1/2), and the half value and full length is approximately 60 Hz.

tional to time elapse, higher frequency stabilization would be obtainable if adopting the estimation of forthcoming drifts from foregoing drifts.

7.2 Summary

We described a report on a $^{40}Ca^{+}$ ion optical frequency standard being under development at NICT. The frequency of the clock transition of $^{40}Ca^{+}$ ions, that is the $^{2}S_{1/2}$–$^{2}D_{5/2}$ transition, was measured based on the definitions of the SI unit of time, and consequently, the absolute frequency was estimated to be 411 042 129 776 395 (±4.8) Hz. The relative uncertainty amounted to 1.2×10^{-14}. Moreover, long-term frequency drift of the clock laser were compensated with the clock transition, and as the result of measuring frequency stability, a stability of 5×10^{-15} was obtained at an averaging time of over 100 seconds. And, in an attempt to ensure a better accuracy and stability, we developed the ion trap equipped with the magnetic shield. The shielding factor of the shield was over 25 at around 50 Hz, which could reduce the full width at half maximum of the clock transition spectrum down to some 60 Hz. At present, we are making preparations for measuring transition frequencies with uncertainties of the 10^{-15} level, and planning for frequency comparisons with strontium atoms or other kinds of ions in future.

References

1 H. Dehmelt, “Mono-Ion Oscillator as Potential Ultimate Laser Frequency Standard, ” IEEE Trans. Instrum. Meas., IM–31, pp. 83–87, 1982.

2 S. Urabe. in “Frontiers In Modern Physics,” edited by Y. Outsuki (Kyoritsu, Tokyo, 2000), Vol. 3, pp. 3–65. (in Japanese)

3 C.-W. Chou, D. B. Hume, J. C. J. Koelemeij, D. J. Wineland, and T. Rosenband, “Frequency Comparison of Two High-Accuracy Al^{+} Optical Clocks,” Phys. Rev. Lett., Vol. 104, 070802, 2010.

4 K. Matsubara, K. Hayasaka, Y. Li, H. Ito, S. Nagano, M. Kajita, and M. Hosokawa, “Frequency Measurement of Optical Clock Transition of $^{40}Ca^{+}$ Ions with an Uncertainty of 10^{-14} Level,” Appl. Phys. Express, Vol. 1, 067011, 2008.

5 H. S. Margolis, G. P. Barwood, G. Huang, H. A. Klein, S. N. Lea, K. Szymaniec, and P. Gill, “Hertz-Level Measurement of Optical Clock Frequency in a Single $^{88}Sr^{+}$ Ion,” Science, Vol. 306, pp. 1355–1358, 2004.

6 C. Tamm, S. Weyers, B. Lipphardt, and E. Peik, ”Stray-Field-Induced Quadrupole Shift and Absolute Frequency of the 688-Thz $^{171}Yb^{+}$ Single-Ion Optical Frequency Standard,” Phys. Rev. A, Vol. 80, 043403, 2009.

7 T. Rosenband, D. B. Hume, P. O. Schmidt, C. W. Chou, A. Brusch, L. Lorini, W. H. Oskay, R. E. Drullinger, T. M. Fortier, J. E. Stalnaker, S. A. Diddams, W. C. Swann, N. R. Newbury, W. M. Itano, D. J. Wineland, and J. C. Bergquist, ”Frequency Ratio of Al^{+} and Hg^{+} Single-Ion Optical Clocks; Metrology at the 17th Decimal Place,” Science, Vol. 319, pp. 1808–1812, 2008.

8 T. Liu, Y. H. Wang, R. Dumke, A. Stejskal, Y. N. Zhao, J. Zhang, Z. H. Lu, L. J. Wang, T. Becker, and H. Walther, “Narrow Linewidth Light Source for an Ultraviolet Optical Frequency Standard,” Appl. Phys. B, Vol. 87, pp. 227–232, 2007.

9 http://www.bipm.org/cc/CIPM/Allowed/98/REC_CIPM2009_C2_LIST_OF_ST_FREQUENCIES_18_DEC_2009.pdf

10 P. K. Ghosh, “Ion Traps,” Oxford University Press, 1995.

11 H. Ishijima, K. Fukuda, K. Matsubara, and M. Hosokawa, “Production of 423-nm Second-Harmonic Generation Light Beam Using pp-KTP Crystal,” The Review of Laser Engineering, Vol. 35, pp. 273–276, 2007. (in Japanese)
12 K. Matsubara, S. Uetake, H. Ito, Y. Li, K. Hayasaka, and M. Hosokawa, “Precise Frequency-Drift Measurement of Extended-Cavity Diode Laser Stabilized with Scanning Transfer Cavity,” Jpn. J. Appl. Phys., Vol. 44, pp. 229–230, 2005.
13 Y. Li, S. Nagano, K. Matsubara , R. Kojima, M. Kumagai, H. Ito, Y. Koyama, and M. Hosokawa, “Development of an Ultra-Narrow Line-Width Clock Laser,” Special issue of this NICT Journal, 3-5, 2010.
14 Y. Li, S. Nagano, K. Matsubara, H. Ito, M. Kajita, and M. Hosokawa, “Narrow-Line and Frequency Tunable Diode Laser System for S–D Transition of Ca^+ Ions,” Jpn. J. Appl. Phys., Vol. 47, pp. 6327–6332, 2008.
15 L.-S. Ma, Z. Y. Bi, A. Bartels, L. Robertsson, M. Zucco, R. S. Windeler, G. Wilpers, C. Oates, L. Hollberg, and S. A. Diddams, “Optical Frequency Synthesis and Comparison with Uncertainty at the 10^{-19} Level,” Science, Vol. 303, pp. 1843–1845, 2004.
16 C. F. Roos, M. Chwalla, K. Kim, M. Riebe, and R. Blatt, “Designer Atoms for Quantum Metrology,” Nature, Vol. 443, pp. 316–319, 2006.
17 M. Kumagai, H. Ito, M. Kajita, and M. Hosokawa, “Evaluation of Caesium Atomic Fountain NICT-CsF1,” Metrologia, Vol. 45, pp. 139–148, 2008.
18 M. Kajita, Y. Li, K. Matsubara, K. Hayasaka, and M. Hosokawa, “Prospect of Optical Frequency Standard Based on a $^{43}Ca^+$ Ion,” Phys. Rev. A, Vol. 72, 043404, 2005.
19 S. Nagano, H. Ito, Y. Li, K. Matsubara, and M. Hosokawa, “Stable Operation of Femtosecond Laser Frequency Combs with Uncertainty at the 10^{-17} Level toward Optical Frequency Standards,” Jpn. J. Appl. Phys., Vol. 48, 042301, 2009.
20 http://www.bipm.org/jsp/en/TimeFtp.jsp?TypePub=publication
21 Y. Hanado,” A generation system of Japan Standard Time with high reliability and accuracy,” Oyo Butsuri, Vol. 76, No. 6, pp. 632–635, 2007. (in Japanese)
22 M. Chwalla, J. Benhelm, K. Kim, G. Kirchmair, T. Monz, M. Riebe, P. Schindler, A. S. Villar, W. Hänsel, C. F. Roos, R. Blatt, M. Abgrall, G. Santarelli, G. D. Rovera, and Ph. Laurent, “Absolute Frequency Measurement of the $^{40}Ca^+$ $4s^2S_{1/2}$–$3d^2D_{5/2}$ Clock Transition,” Phys. Rev. Lett. Vol. 102, 023002, 2009.
23 J. E. Bernard, L. Marmet, and A. A. Madej, “A Laser Frequency Lock Referenced to a Single Trapped Ion,” Opt. Commun. Vol. 150, pp. 170–174, 1998.
24 M. Kajita, Y. Koyama, and M. Hosokawa, “Fundamentals of Time and Frequency,” Special issue of this NICT Journal, 2-1, 2010.

(Accepted Oct. 28, 2010)

MATSUBARA Kensuke, *Ph.D.*

Senior Researcher, Space-Time Standards Group, New Generation Network Research Center

Optical Frequency Standards, Laser Spectroscopy

LI Ying, *Ph.D.*

Senior Researcher, Space-Time Standards Group, New Generation Network Research Center

Optical Frequency Standards, Laser Physics

NAGANO Shigeo, *Ph.D.*

Senior Researcher, Space-Time Standards Group, New Generation Network Research Center

Optical Frequency Standards, Space-Time Measurements

KOJIMA Reiko, *Ph.D.*

Space-Time Standards Group, New Generation Network Research Center

Atomic Frequency Standards, Optical Frequency Standards

KAJITA Masatoshi, *Ph.D.*

Senior Researcher, Space-Time Standards Group, New Generation Network Research Center

Atomic Molecular Physics, Frequency Standard

ITO Hiroyuki, *Ph.D.*

Senior Researcher, Space-Time Standards Group, New Generation Network Research Center

Atomic Frequency Standard, Optical Frequency Standards

HAYASAKA Kazuhiro, *Ph.D.*

Senior Researcher, Quantum ICT Group, New Generation Network Research Center

Quantum Information Science, Quantum Optics, Quantum Electronics

HOSOKAWA Mizuhiko, *Ph.D.*

Executive Director, New Generation Network Research Center

Atomic Frequency Standards, Space-Time Measurements